

# Surface Tension and Contact Angle Modelling in Multiphase Lagrangian Differencing Dynamics

Manigandan Paneer<sup>1,2</sup>, Josip Bašić<sup>1</sup>, Damir Sedlar<sup>1</sup> Chong Peng<sup>3</sup>

<sup>1</sup>Faculty of Electrical Engineering, Mechanical Engineering and Naval Architecture, University of Split,  
Ruđera Boškovića 32, 21000, Split, Croatia

<sup>2</sup>Engineering Software Steyr GmbH, Berggasse 35, 4400, Steyr, Austria

<sup>3</sup>School of Civil Engineering, Southeast University, Nanjing 211189, China  
manigandan.paneer.00@fesb.hr

**Abstract** – Surface tension, wetting, and contact line dynamics are critical to understanding flows involving interactions between different phases, such as liquid-liquid, liquid-gas, and liquid-solid interfaces. Accurately capturing the effects of surface tension and contact angle hysteresis is essential for enhancing simulation fidelity. This paper presents a methodology that integrates surface tension and contact angle force models within the Multiphase Lagrangian Differencing Dynamics (MP-LDD) framework. The pressure jump due to surface tension and the mobility of the contact angle are implicitly incorporated into the pressure equation using the Young-Laplace equation, yielding a good initial guess in the pressure calculation to improve the stability and convergence. Simultaneously, the corresponding volumetric force is integrated into the velocity equation, providing a comprehensive and accurate representation of interfacial dynamics. The MP-LDD framework focuses on the immediate vicinity of the interface, enabling sharper and more precise calculations of surface interactions without relying on ghost particles or complex extrapolations. The approach achieves faster computations by leveraging the dynamic contact angle (DCA) model without curvature calculations and eliminates instabilities caused by abrupt curvature changes. Additionally, the second-order consistency of MP-LDD enhances predictive accuracy. The direct operation on surface meshes allows precise identification of solid boundaries and accurate application of forces at the triple point. Validation against benchmark cases demonstrates the robustness and effectiveness of the proposed methodology in simulating complex multiphase flow scenarios, establishing it as a reliable and efficient tool for interfacial flow simulations.

**Keywords:** Surface tension, contact angle, MP-LDD, interracial dynamics

## 1. Introduction

Surface tension plays a fundamental role in multiphase flow simulations, influencing interface dynamics across various fluid systems. Several computational methods have been developed to model surface tension effects efficiently. The Continuum Surface Force (CSF) method treats surface tension as a distributed force across the interface, facilitating large-scale simulations without explicit interface tracking [1]. Sharp interface methods directly impose the Young-Laplace equation, ensuring precise pressure jumps for applications in droplet dynamics and bubble formation [2]. The Ghost Fluid Method (GFM) enforces jump conditions using ghost cells, maintaining sharp property representation while minimizing numerical errors [3]. Diffuse Interface Models (DIM) represent the interface as a continuous transition between phases, effectively capturing capillary waves and phase separation without explicit tracking [4]. The Lattice-Boltzmann Method (LBM) incorporates surface tension via particle interactions, making it particularly useful for porous media and microfluidic applications [5]. Additionally, Smoothed Particle Hydrodynamics (SPH) employs a meshless framework to compute surface tension forces, ideal for scenarios with significant interfacial deformation, such as free-surface flows [6]. Dynamic wetting behavior is another critical aspect of multiphase systems, often described through Dynamic Contact Angle (DCA) models. These models extend Young's equation (1805), which defines equilibrium contact angles [7], and Laplace's formulation (1806) for capillary action and pressure differences across curved interfaces [8]. The concept of contact angle hysteresis, introduced by Harkins & Jordan (1930), accounts for variations between advancing and receding angles [9], while Blake & Haynes (1969) linked dynamic angles to interfacial kinetics [10]. Subsequent developments, including the Cox-Voinov law (1976) [12], Tanner's correlation (1979) [13], and Kistler's extension (1993) [14], refined the relationship between velocity and contact angle changes. Advanced models, such as Shikhmurzaev's phenomenological approach (1997) [15], Yokoi et al.'s regime-based framework (2009) [17], and Snoeijer & Andreotti's contact line friction model (2013) [18], further enhance

wetting predictions. More recent studies, including Ludwicki et al. (2022) [19], focus on contact-line mobility, improving dynamic wetting simulations.

This paper presents a methodology for integrating surface tension and contact angle models within the MP-LDD framework [20, 21, 22]. By incorporating these forces into the pressure and velocity equations, the approach enhances simulation accuracy and stability. Surface tension effects are handled via the Young-Laplace equation, ensuring smooth pressure gradients, while volumetric forces is incorporated into the velocity equation, providing a comprehensive representation of interfacial dynamics. The use of the dynamic contact angle (DCA) model eliminates curvature calculations, boosting efficiency and preventing instabilities. The MP-LDD framework maintains a sharp interface without additional computational overhead, offering a reliable and efficient solution for complex multiphase flow simulations with second-order consistency [20, 21, 22].

## 2. Governing Equations

The Navier-Stokes equations governing incompressible fluids are expressed as follows:

$$\nabla \cdot \mathbf{u} = 0 \quad (1)$$

$$\frac{D\mathbf{u}}{Dt} = \frac{-\nabla p}{\rho} + \nu \nabla^2 \mathbf{u} + \mathbf{g} + \frac{1}{\rho} \mathbf{F}_{s+d} \quad (2)$$

where,  $D/Dt$  is a material derivative, also known as the convective or substantial derivative,  $\mathbf{u}$  represents the velocity field,  $\rho$  is the fluid density,  $p$  denotes the pressure,  $\nu$  is the kinematic viscosity,  $\mathbf{g}$  stands for acceleration due to gravity and  $\mathbf{F}_{s+d}$  signifies the force due to surface tension plus dynamic contact angle per unit volume. The continuity  $\nabla \cdot \mathbf{u} = 0$  ensures the incompressibility of the fluid, indicating that there are no sources or sinks within the fluid. The Momentum Equation (2) is based on the Lagrangian perspective, accounts for pressure gradients, viscous diffusion, gravitational forces, and surface tension forces.

Solving the Navier-Stokes Equation (2) for incompressible flow involves determining both the pressure and velocity fields within a discretized computational domain. The pressure field is typically computed using the Pressure Poisson Equation (PPE) as below [20, 21]:

$$\nabla \cdot \left( \frac{\nabla p}{\rho} \right) = -\nabla \cdot \frac{D\mathbf{u}}{Dt} \quad (3)$$

The velocity field is typically computed as below [20, 21]:

$$\frac{D\mathbf{u}}{Dt} = \frac{-\nabla p}{\rho} + \nu \nabla^2 \mathbf{u} + \mathbf{g} + \frac{1}{\rho} \mathbf{F}_{s+d} \quad (4)$$

Pressure and velocity equations are solved with MP-LDD discretization, and the gradient variable Laplacian approximation are given by [22]:

$$\langle \nabla f \rangle_i = \mathbf{B}_i \sum_j W_{ij} \mathbf{x}_{ij} (f_j - f_i) \quad (5)$$

$$\langle \nabla \cdot (\varphi \nabla f) \rangle_i = \frac{2d \sum_j L_{ij} \left( \frac{\varphi_i + \varphi_j}{2} \right) (f_j - f_i)}{\sum_j L_{ij} \|\mathbf{x}_{ij}\|^2} \quad (6)$$

Where,  $L_{ij} = W_{ij} (1 - \mathbf{x}_{ij} \cdot \mathbf{B}_i \mathbf{o}_i)$ ,  $f$  is the function,  $\mathbf{B}_i$  is renormalised tensor,  $\mathbf{o}_i$  is offset vector,  $\mathbf{x}_{ij}$  is distance vector between point ( $i$ ) and ( $j$ ),  $W_{ij}$  is weight function, and  $d$  is dimension of the problem. One of the advantages of the Lagrangian Differencing Dynamics (LDD) approach is that it operates directly on surface meshes. In this method, solid points are determined by projecting fluid points that are adjacent to the solid interface. This feature makes it much easier to accurately identify the boundaries of solid objects.

### 3. Surface Tension

Surface tension is a phenomenon that occurs at the interface between two phases. It plays a critical role in multiphase flows, influencing various phenomena such as droplet formation, interface stability, and capillary waves. The effects of surface tension need to be integrated with pressure and velocity calculations. Due to surface tension, there is a pressure jump across the interface, which can be calculated using the Young-Laplace equation. This pressure jump is then added to the pressure term as initial guess while solving pressure, as indicated below:

$$p(i) = \sigma \delta r / \rho_i \quad (8)$$

where,  $\sigma$  is surface tension coefficient and  $\delta r$  is spacing (distance between the points). The pressure value is updated using Equation (6) before calculating the pressure with Equation (3). This update accounts for a pressure jump that is equivalent to the surface tension force at the interface. Additionally, Continuum Surface Tension is applied to incorporate the surface tension force into the velocity equation as below:

$$\mathbf{F}_s = \hat{\mathbf{n}} \sigma \kappa \delta r / \rho \quad (9)$$

where,  $\mathbf{F}_s$  is surface tension force per unit volume,  $\hat{\mathbf{n}}$  is the interfacial normal and  $\kappa$  is curvature. The following is added to the right-hand side of the velocity equation.

$$\mathbf{n} = \frac{\nabla \rho}{\rho_{diff}} ; \hat{\mathbf{n}} = \frac{\mathbf{n}}{\|\mathbf{n}\|} ; \kappa = -(\nabla \cdot \hat{\mathbf{n}}) \quad (10)$$

here,  $\rho_{diff}$  is an absolute difference of the density of two phases and it is constant.

### 4. Contact Angle

Dynamic contact angle ( $\theta_d$ ) is a crucial parameter in modeling wetting phenomena, particularly in multiphase flows involving fluid-solid interfaces. It accounts for both static and dynamic effects, such as surface tension and contact line motion. The dynamic contact angle ( $\theta_d$ ) is determined by incorporating both static and dynamic effects. The radii of the advancing ( $r_A$ ) and receding ( $r_R$ ) contact lines are derived based on the measured maximum dynamic advancing ( $\theta_{mda}$ ) and receding ( $\theta_{mdr}$ ) angle:

$$r_A = \sqrt[3]{\frac{\sin^3(\theta_{mda})}{2-3\cos(\theta_{mda})+\cos(\theta_{mda})}} ; r_R = \sqrt[3]{\frac{\sin^3(\theta_{mdr})}{2-3\cos(\theta_{mdr})+\cos(\theta_{mdr})}} \quad (11)$$

The static contact angle ( $\theta_s$ ) is computed using the weighted contributions of  $r_A$  and  $r_R$ , reflecting the curvature of the interface:

$$\theta_s = \cos^{-1} \left( \frac{r_A \cos(\theta_{mda}) + r_R \cos(\theta_{mdr})}{r_A + r_R} \right) \quad (12)$$

Include the effect of tangential velocity at the contact line, a correction term is added.

$$\Delta\theta = (\theta_{mda} - \theta_{mdr}) \cdot \tanh(\mathbf{u}_{tan} \cdot \mathbf{n}_{tan}) \quad (13)$$

here,  $\mathbf{u}_{tan}$  is tangential velocity to the wall and  $\mathbf{n}_{tan}$  is normal tangential to the wall.  $\Delta\theta$  term adjusts the static contact angle ( $\theta_s$ ) to account for fluid motion. Then the dynamic contact angle ( $\theta_d$ ) is as follow:

$$\theta_d = \theta_s + \Delta\theta \quad (14)$$

Acceleration is based on the difference between target and current angles and converts them to force. Net force in tangential direction per unit volume, due to dynamic contact angle can be computed as below:

$$\mathbf{F}_d = \mathbf{n}_{tan} \cdot DCA_{coef}(\theta_d - \theta_{curr})/\rho \quad (15)$$

where  $\theta_{curr} = \cos^{-1}(-\mathbf{n}_{wall} \cdot \mathbf{n})$  is current angle and  $DCA_{coef} = \sigma \delta r^2$ . The pressure difference at the interface caused by the dynamic contact angle is calculated and added to pressure term as initial guess while solving pressure:

$$p(i) = \sigma \delta r(\theta_d - \theta_{curr})/\rho \quad (16)$$

## 5. Validations

### 5.1. Square droplet - non-equilibrium oscillation

The oscillation of liquid droplets under the influence of surface tension is a fundamental phenomenon in multiphase fluid dynamics. Accurate simulation of this phenomenon is crucial for validating surface tension models in computational frameworks, particularly under simplified conditions where gravity is absent and unbalanced surface tension acts as the primary restoring force [24]. To validate the surface tension model, the oscillation of a square ethanol droplet in a quiescent fluid due to unbalanced surface tension forces is simulated, as illustrated in Figure 1(Left). The ethanol droplet, with a side length of 0.075 m, is surrounded by a low-density fluid with no-slip wall boundaries. The ethanol properties are density ( $797.88 \text{ kg/m}^3$ ) kinematic viscosity ( $1.4 \times 10^{-6} \text{ m}^2/\text{s}$ ) and surface tension coefficient ( $0.02361 \text{ N/m}$ ), while the surrounding fluid has a density ( $1 \text{ kg/m}^3$ ) and a kinematic viscosity ( $1 \times 10^{-5} \text{ m}^2/\text{s}$ ).

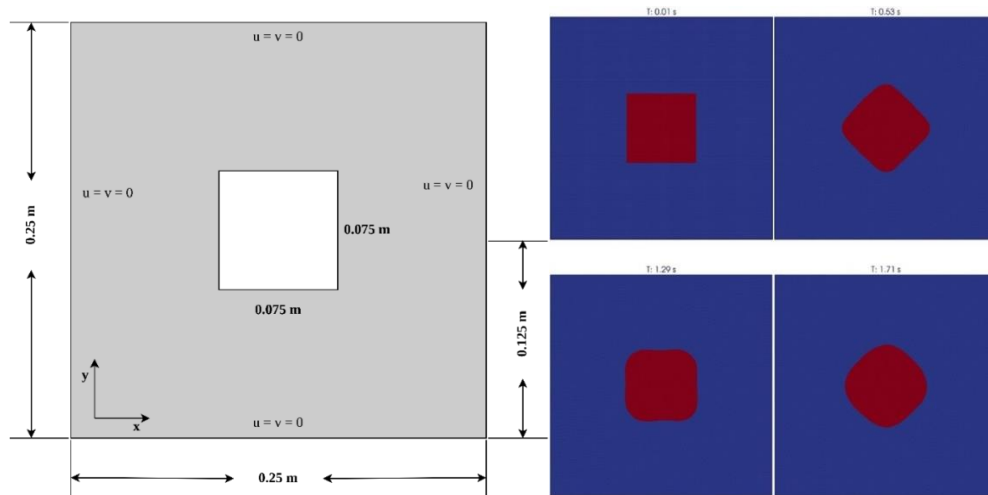


Fig. 1: Case setup (Left) and oscillation result of a square droplet at different time steps (Right).

Square droplet starts oscillating due to the surface tension force. The oscillation frequency is analytically determined, with the corresponding period calculated as 1.299 seconds for the first complete cycle. This result closely aligns with the numerical method outcomes, as illustrated in Figure 1 (Right) for oscillation mode 4. Such an agreement underscores the accuracy of the implemented surface tension model in predicting droplet oscillation dynamics.

## 5.2. Bubble raising

The bubble rising problem with a high surface tension was replicated based on the study by Hysing et al. [23]. A 2D two fluid static interface test case within a  $1 \times 2$  rectangular domain, featuring a circular region (radius 0.5) centered at (0.5, 0.5) occupied by fluid 2, while the surrounding region is filled with fluid 1. No-slip boundary conditions are applied at the top and bottom walls, and horizontal velocity is enforced on the side walls. Fluid properties are mentioned in the Table 1.

Table 1: Fluid parameters used in the simulation

$\rho_1(\text{kg/m}^3)$	$\rho_2(\text{kg/m}^3)$	$\mu_1(\text{Pa.s})$	$\mu_2(\text{Pa.s})$	$g(\text{m/s}^2)$	$\sigma(\text{N/m})$
1000	100	10	1	0.98	24.5

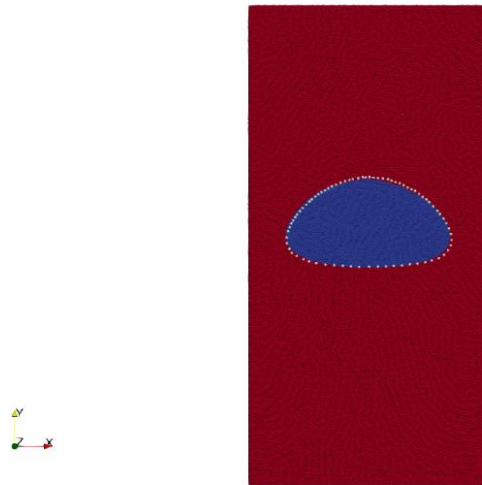


Fig. 2: Comparison of bubble raising with high surface tension is compared with Hysing et al. [20] (White dots) at 3 sec

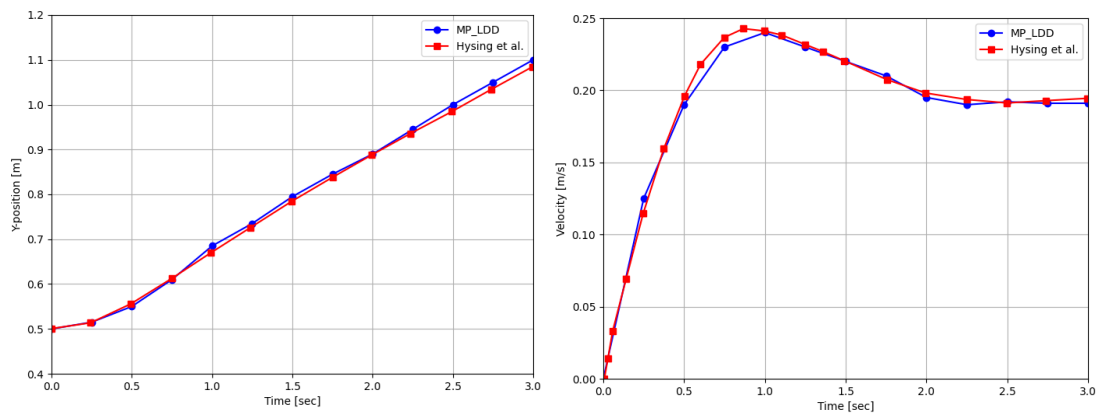


Fig. 3: The movement of center of mass of the bubble at different time steps was compared with Hysing et al [20] (Left) and Raising velocity of the bubble at different time steps was compared with Hysing et al [23] (Right).

The simulation was carried out using the proposed MP-LDD method, and the results were compared with the benchmark data from Hysing et al. to evaluate accuracy and reliability. Figure 2 illustrates the bubble's shape and position at  $t = 3 \text{ s}$ , where the white dots represent the reference data from Hysing et al. The MP-LDD method demonstrates a close match with the benchmark, capturing the sharp interface and maintaining numerical stability. The center of mass of the bubble was tracked over time, and the comparison with Hysing et al. is shown in Figure 3 (Left). The results highlight the accuracy of the MP-LDD method in predicting the upward motion of the bubble, maintaining a consistent alignment with the benchmark values throughout the simulation. The bubble's rising velocity was also examined and compared to the benchmark data, as shown in Figure 3 (Right). The MP-LDD method accurately captures the peak velocity and the subsequent stabilization phase, indicating its capability to handle high surface tension flows while maintaining sharp and stable interfaces. These comparisons validate the robustness and reliability of the MP-LDD method for simulating complex multiphase flows involving surface tension and interface dynamics.

### 5.3 Static contact angle on square droplet

To validate the numerical setup and simulation accuracy, a square ethanol droplet ( $0.06 \text{ m} \times 0.06 \text{ m}$ ) with a density of  $\rho_d = 797.88 \text{ kg/m}^3$  and surface tension  $\sigma = 0.02361 \text{ N/m}$  was placed in a background fluid of density  $\rho_b = 1.0 \text{ kg/m}^3$  and viscosity  $\mu_d = 1 \text{ e}^{-2} \text{ Pa}\cdot\text{s}$ . The effects of gravity and other external forces were neglected to focus purely on the capillary-driven behaviour of the droplet [24].

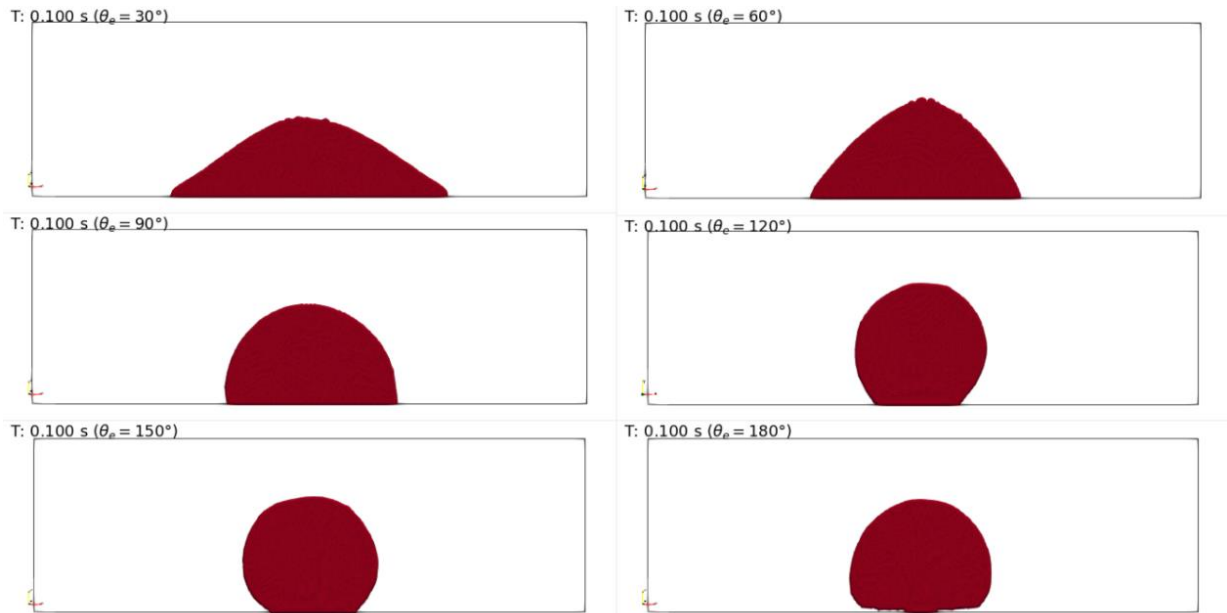


Fig. 4: Equilibrium contact angle study of a square ethanol droplet at different static contact angles ( $30^\circ$  to  $180^\circ$ )

The system was tested for various static contact angles,  $\theta_s$ , ranging from  $30^\circ$  to  $180^\circ$ . The resulting equilibrium configurations of the droplet at  $T=0.1 \text{ s}$  for each contact angle is presented in Figure 4. These configurations were analyzed to confirm the consistency of the contact angle with the imposed  $\theta_s$ , as well as to assess the symmetry and stability of the droplet profile. The droplet deformation was studied under the assumption of a static equilibrium state. The results demonstrate clear adherence to the prescribed contact angles, with the droplet shape transitioning from a flattened dome ( $\theta_s = 30^\circ$ ) to a semicircular ( $\theta_s = 90^\circ$ ), and finally to an increasingly spherical shape ( $\theta_s = 150^\circ$  and  $\theta_s = 180^\circ$ ) as the contact angle increased. These results are consistent with theoretical expectations for static contact angle behavior in the absence of external forces. This validation confirms the reliability of the numerical method in reproducing equilibrium droplet shapes governed by surface tension and contact angle conditions.

## 5.4 Effect of surface tension and Dynamic contact angle

The spreading of semi-water droplets with radius of 0.5 m placed on a surface with gravitational force was studied under three configurations to analyze the effects of surface tension (ST) and dynamic contact angle (DCA): (1) No ST + No DCA, (2) ST + No DCA, and (3) ST + DCA. Figure 5 (Left) explains that the absence of ST and DCA, the droplet spreads maximally with a large footprint and reduced height. Adding ST significantly reduces the spreading length, much smaller than the case with both ST and DCA, which shows a moderately constrained footprint and the highest central height due to additional constraints from contact angle dynamics. Also effect of surface energy of the contact surface. These findings emphasize the critical role of ST and DCA in controlling droplet behavior, with implications for applications in coatings, lubrication, and material science.



Fig. 5: Comparison of Droplet Spreading under Different Configurations of Surface Tension (ST) and Dynamic Contact Angle (DCA) at 0.1 sec (Left) and spread length comparison No ST + No DCA (red), ST + No DCA (blue) and ST + DCA (yellow) (Right).

## 6. Conclusion

In this study, we developed and validated a methodology for integrating surface tension and contact angle force models within the MP-LDD framework. By avoiding curvature calculations in the dynamic contact angle (DCA) model, our approach achieves faster computations and eliminates instabilities caused by abrupt curvature changes. Incorporating surface tension and contact angle dynamics into the pressure and velocity equations resulted in smoother pressure gradients and accurate interfacial dynamics. The second-order consistency of MP-LDD, combined with its focus only on adjacent interface layers and direct surface mesh operations, enabled precise and efficient simulations. Validation against benchmark cases demonstrated the method's effectiveness, establishing it as a reliable tool for simulating complex multiphase flows. Future work will extend this framework to non-Newtonian fluids and dynamic contact line phenomena.

## Acknowledgements

This research was supported by CELTIC-NEXT under project COA-CFD (ID C2021/1-11) and received funding from the European Space Agency (ESA) under project 4000143610/24/NL/MH/rp.

## References

- [1] J. U. Brackbill, D. B. Kothe, and C. Zemach, "A continuum method for modeling surface tension," *J. Comput. Phys.*, vol. 100, pp. 335–354, 1992.
- [2] G. Tryggvason, R. Scardovelli, and S. Zaleski, "Direct Numerical Simulations of Gas–Liquid Multiphase Flows". Cambridge University Press, 2011.
- [3] R. P. Fedkiw, T. Aslam, B. Merriman, and S. Osher, "A non-oscillatory Eulerian approach to interfaces in multimaterial flows (the ghost fluid method)," *J. Comput. Phys.*, vol. 152, pp. 457–492, 1999.
- [4] D. M. Anderson, G. B. McFadden, and A. A. Wheeler, "Diffuse-interface methods in fluid mechanics," *Annu. Rev. Fluid Mech.*, vol. 30, pp. 139–165, 1998.
- [5] X. Shan and H. Chen, "Lattice Boltzmann model for simulating flows with multiple phases and components," *Phys. Rev. E*, vol. 47, no. 3, p. 1815, 1993.
- [6] J. P. Morris, P. J. Fox, and Y. Zhu, "Modeling low Reynolds number incompressible flows using SPH," *J. Comput. Phys.*, vol. 136, pp. 214–226, 2000.
- [7] T. Young, "An essay on the cohesion of fluids," *Phil. Trans. R. Soc. Lond.*, vol. 95, pp. 65–87, 1805.
- [8] P. S. Laplace, "Mécanique Céleste", *Paris: Courcier*, Vol. 4. 1806
- [9] W. D. Harkins and H. F. Jordan, "A method for the determination of surface and interfacial tension from the maximum pull on a ring," *J. Am. Chem. Soc.*, vol. 52, pp. 1751–1772, 1930.
- [10] T. D. Blake and J. M. Haynes, "Kinetics of liquid/liquid displacement," *J. Colloid Interface Sci.*, vol. 30, pp. 421–423, 1969.
- [11] J. F. Joanny and P. G. de Gennes, "A model for contact angle hysteresis," *J. Chem. Phys.*, vol. 81, pp. 552–562, 1984.
- [12] O. V. Voinov, "Hydrodynamics of wetting," *Fluid Dyn.*, vol. 11, pp. 714–721, 1976.
- [13] L. H. Tanner, "The spreading of silicone oil drops on horizontal surfaces," *J. Phys. D: Appl. Phys.*, vol. 12, p. 1473, 1979.
- [14] S. F. Kistler, "Hydrodynamics of wetting," in *Wettability*, Springer, pp. 311–429, 1993.
- [15] Y. D. Shikhmurzaev, "Moving contact lines in liquid/liquid/solid systems," *J. Fluid Mech.*, vol. 334, pp. 211–249, 1997.
- [16] B. A. Nichita, I. Zun and J. R. Thome " A VOF method coupled with a dynamic contact angle model for simulation of two-phase flows with partial wetting," *7th International Conference on Multiphase Flow*, May 30 – June 4, 2010.
- [17] Kensuke Yokoi, Damien Vadillo, John Hinch and Ian Hutchings, " Numerical studies of the influence of the dynamic contact angle on a droplet impacting on a dry surface," *Phys. Fluids*, vol. 21, no. 7, p. 072102, 2009.
- [18] J. H. Snoeijer and B. Andreotti, "Moving contact lines: Scales, regimes, and dynamical transitions," *Annu. Rev. Fluid Mech.*, vol. 45, pp. 269–292, 2013.
- [19] Jonathan M. Ludwicki, Vanessa R. Kern, Joshua McCraney, Joshua B. Bostwick, Susan Daniel, Paul H. Steen. "Material parameter studies for dynamic contact line mobility," *J. Colloid Interface Sci.*, vol. 613, pp. 722–737, 2022.
- [20] Josip Basic, Nastia Degiuli, and Dario Ban, "A class of renormalised meshless Laplacians for boundary value problems," *Journal of Computational Physics*, vol. 354, pp. 269–287, 2018.
- [21] Josip Basic, Nastia Degiuli, Branko Blagojevic, and Dario Ban, "Lagrangian differencing dynamics for incompressible flows," *Journal of Computational Physics*, vol. 462, pp. 111198, 2022.
- [22] Manigandan Paneer, Josip Basic, Damir Sedlar, and Chong Peng, "Multiphase Lagrangian Differencing Dynamics method with sharp interfaces," *Engineering Analysis with Boundary Elements*, vol. 175, pp. 106197, 2025
- [23] Hysing, S., Turek, S., Kuzmin, D., Parolini, N., Burman, E., Ganesan, S., Tobiska, L., 2009. "Quantitative benchmark computations of two-dimensional bubble dynamics," *International Journal for Numerical Methods in Fluids*, 60, 1259-1288.
- [24] Liu, Jie, Koshizuka, Seiichi, Oka, Yoshiaki, 2005. " A hybrid particle-mesh method for viscous, incompressible, multiphase flows," *Journal of Computational Physics*, Volume 202, Issue 1, p. 65-93.